INSTITUT DE FRANCE
Académie des sciences

Comptes Rendus
Mécanique

Radhouane Sghir

Unbalance-induced whirl of a rotor supported by oil-film bearings

Volume 349, issue 2 (2021), p. 371-389

Published online: 7 June 2021

https://doi.org/10.5802/crmeca.83

Les Comptes Rendus. Mécanique *sont membres du*
Centre Mersenne pour l'édition scientifique ouverte
www.centre-mersenne.org
e-ISSN : 1873-7234

Comptes Rendus
Mécanique
2021, 349, nº 2, p. 371-389
https://doi.org/10.5802/crmeca.83

Short paper / *Note*

Unbalance-induced whirl of a rotor supported by oil-film bearings

Radhouane Sghir [a, b]

[a] Laboratory of Mechanical Engineering, National Engineering School of Monastir, University of Monastir, Avenue Ibn Eljazzar, 5019 Monastir, Tunisia

[b] National Engineering School of Sousse, University of Sousse, Sousse Technological Center, Sahloul Belt Road, 4054 Sousse, Tunisia

E-mail: sghirradhoineim@yahoo.fr

Abstract. This paper presents a nonlinear stability analysis of an unbalanced rotor-bearing system using the numerical continuation method and the numerical integration method. In this study, the effect of unbalance on journal motion is highlighted and a relationship is established between the bifurcation diagram of a balanced rotor and that of an unbalanced rotor. The results show that the stable operating speed range, the shaft motion type, the whirl speed and the chaotic motion occurrence depend on the unbalance level, the bearing geometry, the oil viscosity, and the speed range of unstable limit cycles existence.

Keywords. Nonlinear stability analysis, Numerical continuation, Unbalanced rotor, Whirl speed, Chaotic motion, Hydrodynamic forces, Unstable limit cycles.

Manuscript received 26th December 2020, revised 23rd April 2021, accepted 26th April 2021.

1. Introduction

The unbalance force can generate several perturbations on the nonlinear phenomena within the hydrodynamic bearing and it can cause remarkable changes in the stability threshold compared to the balanced rotor. These phenomena can cause the unexpected failure of the bearing rotor system. Thus, the analysis of the imbalance effect on rotor stability and the nature of their movement is necessary for safe and successful system design.

Several investigations have focussed on the nonlinear dynamic analysis of rotating machines supported by hydrodynamic bearings [1–8]. These studies have shown several phenomena that cannot be predicted and explained by linear analysis. The studies reported in [1–4] used the Hopf bifurcation theory to consider periodic oscillations in the vicinity of the critical stability speed for a rotor supported by two plain bearings. These studies have shown that the Hopf point (the linear stability threshold) can bifurcate into stable limit cycles or unstable limit cycles. Stable limit cycles are periodic orbits of amplitude that increase proportionally with speed. The bifurcation of the latter is produced at speeds above the stability threshold speed, while the bifurcation of unstable limit cycles occurs at speeds below the stability threshold speed.

In subsequent research, the numerical continuation method, also known as the path following method was used to predict the solutions of nonlinear differential equation systems as a function of a control parameter [5–8]. Furthermore, continuation methods provide, in addition to the analytical methods used in [1–4], tools to accurately predict the size and shape of limit cycles and their bifurcations. Also, the use of the numerical continuation method in the field of rotor stability analysis made it possible to observe and explain in a suitable manner several nonlinear phenomena such as: the hysteresis phenomenon, the jump phenomenon, and the bi-stability phenomenon [7, 8].

The consideration of the unbalance defect can attribute several phenomena to the movement of the rotor. These phenomena contribute to a radical change in rotor stability. A numerical study [9] has shown that the rotor imbalance is at the origin of subharmonic and super-harmonic movements. The influence of turbulence due to unbalance on the instability of a rotor supported by short symmetric bearings is analyzed in [10]. The study is carried out for different values of the Reynolds number and unbalance. Some articles refer to simple systems like Jeffcott's rotors [11–13] to study some examples of unsynchronized periodic movements. This type of movement arises due to the unbalance force and nonlinear elastic restoring forces. Experimental and numerical integration studies have been conducted by Adiletta [14–17]. These studies have identified the paths that lead the movement of a rigid rotor supported by two short hydrodynamic bearings to chaos. Adiletta determined that the rotor movement changes from a periodic motion to a multi-periodic motion before it becomes chaotic. He also showed that during the chaotic motion, the rotor center follows orbits of variable amplitudes which can cause the failure of the bearing. Vibration caused by friction between rotor and bearing has been studied previously [18–20]. These studies [18, 19] have shown that the friction force and the unbalance force generate several types of vibration within the system such as chaotic, periodic, and quasi-periodic vibrations. Also, these studies have identified the most prevalent routes to chaos in rotor–stator contact systems. The chaotic response of a rigid rotor supported by short hydrodynamic bearings is studied in [21]. This study showed that chaotic motion appears for moderate imbalance values. In addition, the authors found that for higher imbalance values, the rotor response becomes periodic again. The effect of unbalance forces on a rotor supported by ball bearings is investigated using the numerical integration method [22]. The authors conclude that quasi-periodic behavior is a step in the road to chaos. The bifurcation of an unbalanced flexible rotor-bearing system is studied in [23] using short-bearing approximation and numerical integration. Rotor movement has been shown to have several nonlinear phenomena such as jumps, subharmonic motion, and quasi-periodic motion. In [24] the authors study the effects of the seal force, the oil-film force, the rotational speeds and eccentrics of two discs on the instability of the oil film of a rotor-bearing-seal system. Research focuses on the effects of two loading conditions (in-phase unbalances of two discs and out-of-phase unbalances of two discs) on the first and second mode whips. In a similar vein, Ma *et al.* [25, 26] have studied the effect of the eccentric phase difference between two disks on the instability of the oil film using bifurcation diagrams, spectrum cascades, vibration waveforms, orbits, and Poincaré maps. This study shows that the increase in eccentric phase difference leads to an increase in the speed of instability (whip/whirl). In [27], Ma *et al.* used a finite element (FE) model of the overhung rotor system with parallel and angular misalignments considering the nonlinear forces of the oil film and the unbalance exciting force to study the oil-film instability laws in the run-up and run-down processes. These authors have shown that under the perfectly aligned condition, due to the hysteresis effect, the onsets of instability in the run-down process are less than those in the run-up process.

The studies reported in [14–16] are limited to studying the effect of unbalance on the stability of the rotor-bearing system for a specific geometry and loading. Also, in [14–16] the analysis of the imbalance effect on the nature of the movement and on the variation of the stability threshold

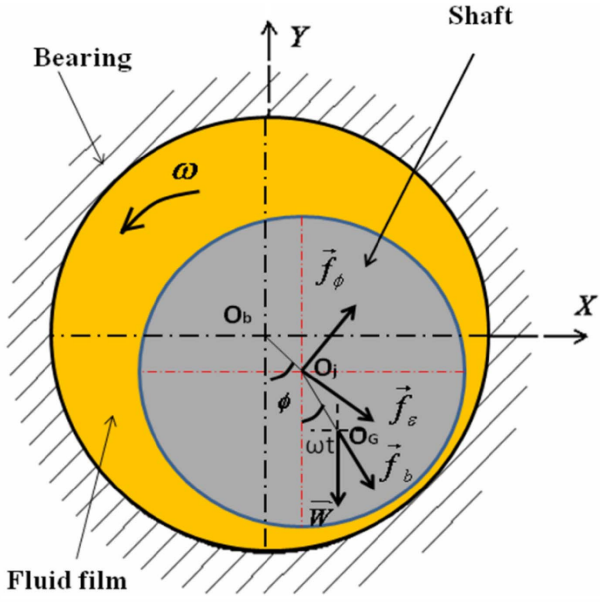

Figure 1. A bearing section that shows the coordinate system and the forces applied to the shaft.

speed compared to a balanced rotor has not been studied. Moreover, in subsequent work, the appearance of chaotic motion and sudden jump for rotor-bearing systems characterized by low oil viscosity or high rotor mass has not been explained. A study using the numerical continuation method and the numerical integration method is essential to analyze the different bifurcations of an unbalanced rotor and to identify the imbalance effect on the rotor-bearing system stability. This study must be performed for a well-chosen variety of the rotor-bearing system geometry to generalize the study and to explain the effect of the system geometry on the dynamic behavior of the rotor.

In this paper, the unbalance effect is introduced by a model of nonlinear differential equations defined in section "Mathematical modeling". The resolution of this system of equations is carried out by two methods: the numerical continuation method and the numerical integration method. These methods are defined in the section "Solving methods". In the "Results" section, the bifurcation diagrams are presented for different unbalance values and for three well-chosen bearing parameters on the bifurcation domains. Also, the nature of movement and the stability threshold speed are predicted for different values of unbalance. In addition, in this section, the effect of unbalance and geometry of the rotor-bearing system on rotor motion and stability threshold speed are investigated and a relationship is established between the occurrence of the chaotic domain, the bearing geometry, reducing the speed of the stability threshold and increasing unbalance. The results are discussed in view of other published numerical and experimental work and conclusions arrived at.

2. Mathematical modeling

Consider a rigid rotor supported symmetrically by two hydrodynamic bearings. The bearings are supposed to be aligned and identical. A section of a bearing is given in Figure 1. The movement of the shaft is described by two degrees of freedom (ε, ϕ), where ε is the eccentricity ratio and ϕ is

the attitude angle. The eccentricity of the shaft center O_j with respect to the bearing center O_b is defined by $e = c\varepsilon$, where c is the radial clearance between the shaft and the bearing.

The position of the shaft gravity center O_G with respect to the shaft rotation center O_j is defined at each moment in polar coordinate by the angular position ωt and the unbalance a. The displacement between these two centers results from a centrifugal force $\vec{f}_b$ of module $|\vec{f}_b| = Ma\omega^2$. This force and the weight of half of the rotor $W = Mg$ are applied to the rotor gravity center. The center of the shaft is provided for each bearing the components of the hydrodynamic force $\vec{f}_\varepsilon$ and $\vec{f}_\phi$.

The system of equations (1) describes the movement of the shaft center. These equations are obtained by applying Newton's second law to the shaft center.

$$\begin{cases} \varepsilon'' - \varepsilon\phi'^2 = \dfrac{\omega^2 a}{c}\cos(\omega t - \phi) + \dfrac{g}{c}\cos\phi + \dfrac{f_\varepsilon}{Mc} \\ \varepsilon\phi'' + 2\varepsilon'\phi' = \dfrac{\omega^2 a}{c}\sin(\omega t - \phi) - \dfrac{g}{c}\sin\phi + \dfrac{f_\phi}{Mc} \end{cases} \tag{1}$$

In the equations of the system (1), the prime ($'$) denotes a derivative with respect to time t, a is the displacement between the shaft gravity center and the shaft rotation center, M is the mass of half the shaft and $\vec{f}_\varepsilon$, $\vec{f}_\phi$ are the components of the fluid film force, respectively in the radial and tangential directions. These latter are obtained by integrating the pressure distribution in the oil films derived from the solutions of Reynolds equation using the short-bearing theory and the pi-film Sommerfeld boundary condition. Expressions of $\vec{f}_\varepsilon$ and $\vec{f}_\phi$ are given by (2) and (3) as a function of (ε, ϕ) and $(\dot{\varepsilon}, \dot{\phi})$, [28].

$$f_\varepsilon = -\frac{\mu R L^3}{2c^2}\left[\pi\dot{\varepsilon}\frac{(1+2\varepsilon^2)}{(1-\varepsilon^2)^{5/2}} + 2\varepsilon^2\frac{(\omega - 2\dot{\phi})}{(1-\varepsilon^2)^2}\right] \tag{2}$$

$$f_\phi = \frac{\mu R L^3}{2c^2}\left[\frac{4\dot{\varepsilon}\varepsilon}{(1-\varepsilon^2)^2} + \frac{\pi\varepsilon}{2}\frac{(\omega - 2\dot{\phi})}{(1-\varepsilon^2)^{3/2}}\right] \tag{3}$$

where μ is the lubricant viscosity, R is the journal radius, L is the bearing length and g is the gravitational acceleration.

The division of each term in the system equations (1) by ω^2 and the derivation with respect to nondimensional time $\tau = \omega t$ allow to obtain the following system of equations:

$$\begin{cases} \ddot{\varepsilon} = \varepsilon\dot{\phi}^2 + \overline{a}\cos(\tau - \phi) + \dfrac{1}{\overline{\omega}^2}\cos\phi + \overline{f_\varepsilon} \\ \ddot{\phi} = \dfrac{2\dot{\varepsilon}\dot{\phi}}{\varepsilon} + \dfrac{\overline{a}}{\varepsilon}\sin(\tau - \phi) + \dfrac{\sin\phi}{\overline{\omega}^2\varepsilon} + \dfrac{\overline{f_\phi}}{\varepsilon} \end{cases} \tag{4}$$

where $(\cdot) = \mathrm{d}/\mathrm{d}\tau = \mathrm{d}/\omega\,\mathrm{d}t$ denotes a derivative with respect to nondimensional time τ, the nondimensional fluid film force components are defined as: $\overline{f_\varepsilon} = f_\varepsilon/Mc\omega^2$ and $\overline{f_\phi} = f_\phi/Mc\omega^2$, the dimensionless rotor speed is defined by $\overline{\omega} = \omega/\sqrt{g/c}$ and the dimensionless unbalance is defined by $\overline{a} = a/c$.

Using the state variables $x_1 = \varepsilon$, $x_2 = \phi$, $x_3 = \dot{\varepsilon}$, $x_4 = \dot{\phi}$, the system of equation (4) may be converted into the following four first-order differential equations:

$$\begin{cases} \dot{x}_1 = x_3 \\ \dot{x}_2 = x_4 \\ \dot{x}_3 = x_1 {x_4}^2 + \overline{a}\cos(\tau - x_2) + \dfrac{\cos x_2}{\overline{\omega}^2} - \dfrac{\Gamma}{\overline{\omega}}\left[\pi x_3\dfrac{(1+2{x_1}^2)}{(1-{x_1}^2)^{5/2}} + 2{x_1}^2\dfrac{(1-2x_4)}{(1-{x_1}^2)^2}\right] \\ \dot{x}_4 = \dfrac{2x_3x_4}{x_1} + \dfrac{\overline{a}}{x_1}\sin(\tau - x_2) - \dfrac{\sin x_2}{\overline{\omega}^2 x_1} - \dfrac{\Gamma}{x_1\overline{\omega}}\left[\dfrac{\pi(1-2x_4)x_1}{2(1-{x_1}^2)^{1.5}} + \dfrac{4x_3x_1}{(1-{x_1}^2)^2}\right]. \end{cases} \tag{5}$$

The system of equations (5) is of the form:

$$\dot{X} = f(X, \tau, \overline{\omega}, \Gamma, \overline{a})$$

with $X = (\varepsilon, \phi, \dot{\varepsilon}, \dot{\phi})^T$.

The above nonlinear system of equations depends on three nondimensional parameters: the bearing parameter $\Gamma = \mu R L^3 / 2Mc^{2.5} g^{0.5}$, the dimensionless rotor speed $\overline{\omega}$ and the dimensionless unbalance $\overline{a}$.

The steady state equilibrium position $X_s = (x_{1s}, x_{2s}, x_{3s}, x_{4s}) = (\varepsilon_s, \phi_s, \dot{\varepsilon}_s, \dot{\phi}_s)$, can be found analytically for $\overline{a} = 0$ by solving the system of equations $\dot{X} = f(X_s, \overline{\omega}, \Gamma) = 0$.

The resulting equations for the static equilibrium position of the system are:

$$\begin{cases} \dfrac{x_{1s}\sqrt{16x_{1s}^2 + \pi^2(1 - x_{1s}^2)}}{(1 - x_{1s}^2)^2} = \dfrac{\varepsilon_s\sqrt{16\varepsilon_s^2 + \pi^2(1 - \varepsilon_s^2)}}{(1 - \varepsilon_s^2)^2} = \dfrac{2}{\Gamma\overline{\omega}} \\ x_{2s} = \phi_s = \tan^{-1}\left(\dfrac{\pi\sqrt{(1 - x_{1s}^2)}}{4x_{1s}}\right) = \tan^{-1}\left(\dfrac{\pi\sqrt{(1 - \varepsilon_s^2)}}{4\varepsilon_s}\right) \\ x_{3s} = \dot{\varepsilon}_s = 0 \\ x_{4s} = \dot{\phi}_s = 0 \end{cases} \tag{6}$$

From (6), the static equilibrium position of the journal center (ε_s, ϕ_s) is determined for a given bearing parameter Γ and a dimensionless rotor speed $\overline{\omega}$. This position is used as an initial solution for the solving methods.

3. Solving methods

Solving the system of differential equations (5) can be performed by numerical integration or numerical continuation. The latter allows a rapid analysis of the speed range, but it is difficult to apply it to the case of an unbalanced rotor $\overline{a} \neq 0$. Consequently, the numerical continuation method will be used in the case of a balanced rotor and the numerical integration method for the case of an unbalanced rotor.

3.1. *Numerical continuation method*

Generally, the numerical continuation method is applied to systems of nonlinear differential equations that are written in the form $\dot{\vec{X}} = f(\vec{X}, \lambda)$, where $\vec{X}$ is a vector of variables and λ the parameter of the system equations. The concept of continuation occurs when, starting from a solution $\vec{X}_0$ determined by solving the system of equations $\dot{\vec{X}} = f(\vec{X}, \lambda) = 0$ for a given value of the parameter λ_0, we are interested to approximately determine its future when the parameter λ changes [29, 30].

From a given solution $(\vec{X}_0, \lambda_0)$ and under the condition of the regularity and the continuity of the domain there exists in the general case a branch of unique solutions, that is to say a single continuum of solutions $(\vec{X}(\lambda), \lambda)$. Therefore, the continuation consists of calculating the solution branch of a system of nonlinear differential equations from an initial solution point.

The MATCONT toolbox [31, 32] is chosen for use in this paper as an interactive tool for the continuation of the branches of the equilibrium points and limit cycles. In addition, the toolbox is used to monitor and detect the bifurcation of the branches of solutions. The MATCONT toolbox is an open source and shareware collection of numerical algorithms implemented in the Matlab language for the continuation and bifurcation of nonlinear differential equations.

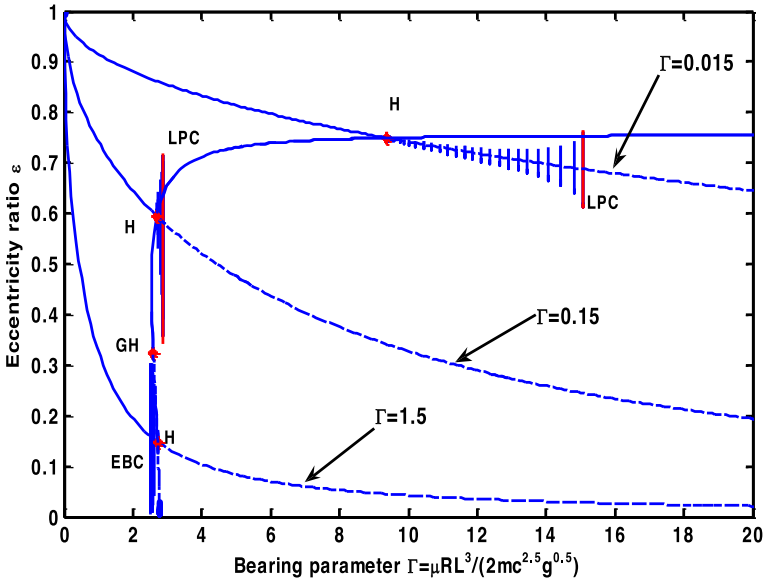

Figure 2. Bifurcation diagrams for a balanced rotor for three selected bearing parameters $\Gamma = 0.015, 0.15$ and 1.5.

3.2. *Numerical integration method*

The numerical integration method is considered a simple and direct method to show the orbit of motion for an unbalanced rotor. To apply the numerical integration method, the equations of a nonlinear system (5) are integrated from a selected initial state. The trajectory of the shaft center can thus be determined. Depending on the initial state and the system parameters, the trajectory of the rotor center can converge to a stable orbit if the initial point belongs to the basin of attraction of a stable solution. However, the trajectory diverges in the case where the initial position is outside the basin of attraction of a stable solution.

Matlab software proposes the functions ode45 based on the Runge–Kutta method for the resolution of ordinary differential equations by numerical integration. These functions allow solving differential equations by integrating system $\dot{X} = f(t, X, \lambda)$ between t_0 and t_f starting from an initial condition X_0. The ode45 function was chosen after several tests to be a basic function for Matlab programs developed in this paper.

4. Results

The purpose of the investigation is to determine the effect of unbalance on the shaft center movement at different rotation speeds and for representative geometries of the bearing ($\Gamma = 0.015, 0.15, 1.5$). In this study, the bearing parameter Γ and the dimensionless unbalance $\overline{a}$ are selected and the dimensionless rotor speed is used as a control parameter. To analyze the effect of unbalance, a balance rotor $\overline{a} = 0$ is used in this study as a reference. In this case, the bifurcation diagrams are determined using the numerical continuation as explained in detail in [7] and [8]. The nondimensional unbalance is then increased progressively by a step of 0.05 from $\overline{a} = 0$ to $\overline{a} = 0.2$.

Figure 2 shows the bifurcation diagrams of a balanced rotor $\overline{a} = 0$, for three bearing parameters $\Gamma = 0.015, 0.15, 1.5$. These diagrams are determined by numerical continuation. The continuation of an equilibrium position for the case of an equilibrium rotor makes it possible to determine

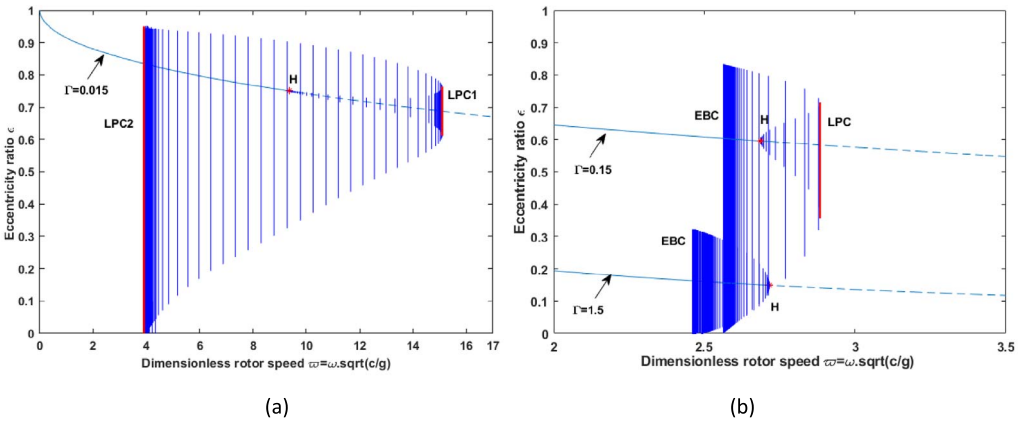

Figure 3. Bifurcation diagrams for a balanced rotor: (a) bifurcation diagrams for $\Gamma = 0.015$, (b) bifurcation diagrams for $\Gamma = 0.15$ and $\Gamma = 1.5$.

the branches of the equilibrium positions. These positions are stable for a rotor speed lower than the stability threshold speed, $\overline{\omega} < \overline{\omega}_H$, for which the branches of the equilibrium points are given in solid lines. For $\overline{\omega} > \overline{\omega}_H$, equilibrium point branches are unstable and presented as dashed lines. Here $\overline{\omega}_H$ denotes the linear stability threshold speed. The index H is used here because this threshold speed occurs at a Hopf bifurcation. This bifurcation is detected when all the eigenvalues of the Jacobian matrix of the system (5) have negative real parts except for a conjugate pair that is purely imaginary [31].

Once a Hopf bifurcation point is located on the branch of equilibrium positions at a rotor speed $\overline{\omega}_H$, a branch of stable or unstable limit cycles can be extended from the Hopf point by numerical continuation. Typically, the amplitude of the limit cycles increases as the control parameter $\overline{\omega}$ increases. The limit cycles are stable for a supercritical Hopf bifurcation and for the control parameter $\overline{\omega} > \overline{\omega}_H$. On the other hand, the limit cycles are unstable for a subcritical Hopf bifurcation and for $\overline{\omega} < \overline{\omega}_H$.

The Hopf point continuation using two control parameters (ω, Γ) allows to draw the linear stability boundary. This boundary is divided into a supercritical Hopf bifurcation domain and a subcritical Hopf bifurcation domain by the generalized Hopf point bifurcation (GH) ($\overline{\omega}_{\mathrm{GH}} = 2.6, \Gamma_{\mathrm{GH}} = 0.588$). The stability threshold is the curve joining the Hopf bifurcation points. It is indicated in Figure 2 by a solid line for the supercritical Hopf bifurcation and a dotted line for the subcritical Hopf bifurcation.

From Figure 2, we notice that the Hopf bifurcation is supercritical for $\Gamma = 0.015$ and 0.15 and subcritical for $\Gamma = 1.5$. For a balanced rotor, the limit cycles can undergo the Limit Point of Cycle bifurcation (LPC) as long as the limit of the eccentricity $\varepsilon = 1$, is not reached. This bifurcation is also known in the literature as the fold bifurcation or saddle node [4]. Following Hopf supercritical bifurcation, the system undergoes two successive LPC bifurcations for $\Gamma = 0.015$ and a single LPC bifurcation for $\Gamma = 0.15$ as shown respectively in Figures 3(a) and (b). For $\Gamma = 1.5$, no LPC bifurcation is found as shown in Figure 3(b). The LPC bifurcation is met at the rotor speed noted $\overline{\omega}_{\mathrm{LPC}}$. The speed range $\overline{\omega}_{\mathrm{LPC1}} - \overline{\omega}_{\mathrm{LPC2}} = 11.18$, $\overline{\omega}_{\mathrm{LPC1}} - \overline{\omega}_{\mathrm{EBC}} = 0.28$ and $\overline{\omega}_H - \overline{\omega}_{\mathrm{EBC}} = 0.26$ represent the domains of existence of unstable limit cycles (hysteresis domains) respectively for $\Gamma = 0.015$, $\Gamma = 0.15$ and $\Gamma = 1.5$. A great disturbance of the system in this speed range, which leads the rotor center to oscillations of amplitudes greater than those of the unstable limit cycles, can make the rotor jump at a large limit cycle movement as reported in [33]. In Figure 3(b), $\overline{\omega}_{\mathrm{EBC}}$ represents the speed of the end of unstable limit cycles bifurcation.

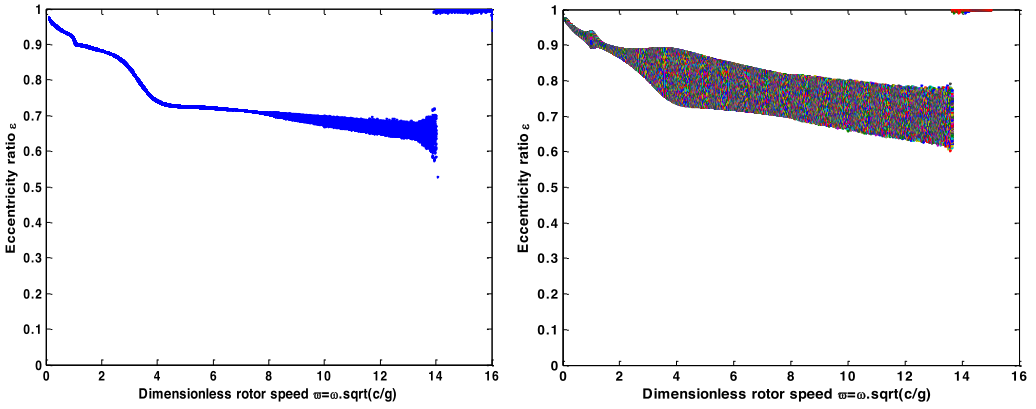

Figure 4. Bifurcation diagram and motion graph for $\Gamma = 0.015$ and $\overline{a} = 0.05$: (a) bifurcation diagram, (b) motion graph.

For the supercritical bifurcation domain, it is generally considered acceptable to operate the rotor with small stable limit cycles so that the stable speed range is extended. In this case, the range between the linear stability boundary and the LPC bifurcation defines an additional margin of stability for rotor operation. Therefore, the stability threshold speed is defined by $\overline{\omega}_{\mathrm{LPC}}$. We can notice that the speed range $\overline{\omega}_{\mathrm{LPC}} - \overline{\omega}_H$ monotonically decreases when approaching $\Gamma = 0.588$ and it disappears totally in the subcritical domain. This speed range is approximately 62% of $\overline{\omega}_H$ at $\Gamma = 0.015$ and 10% of $\overline{\omega}_H$ at $\Gamma = 0.15$. For the subcritical bifurcation domain the stability threshold speed is defined by $\overline{\omega}_H$.

In the following, the effect of unbalance is investigated for the three bearing parameters previously defined. For each bearing parameter, the unbalance is gradually increased by a step of $\Delta\overline{a} = 0.05$. Figure 4 shows the bifurcation diagram and the motion graph for $\Gamma = 0.015$ and $\overline{a} = 0.05$. These diagrams show that the shaft movement is T-periodic for $\overline{\omega} < 7.85$. For $7.85 < \overline{\omega} < 13.9$ the movement of the rotor center becomes quasi-periodic. The quasi-periodicity of movement is justified by the closed curve of the Poincaré map and the rotor center orbit (Figure 5(a)). When the rotor speed $\overline{\omega} > 13.9$, the orbits become 2T-periodic with large oscillations corresponding to $\varepsilon(t)$ close to one (Figure 5(b)).

The movement presented in Figure 4 follows very closely the bifurcation diagram of a balanced rotor (Figure 2). The major difference is that the movement becomes periodic instead of a stable motion around a fixed point for speeds below Hopf's bifurcation speed. It can also be deduced from this figure that the effect of the unbalance is very low on the stability threshold speed where the movement passes to large oscillations with possible friction between the shaft and the bearing (whirl). This speed goes from $\overline{\omega} = 15.09$ for $\overline{a} = 0$ to $\overline{\omega} = 13.99$ for $\overline{a} = 0.05$. These results imply that for a low bearing parameter, safe operation is possible up to relatively high rotor speed, as long as the unbalance is kept under strict control $\overline{a} \leq 0.05$.

When the unbalance is increased to $\overline{a} = 0.1$, the diagrams presented in Figure 6 show the appearance of multi-period movements (2T-periodic, 3T-periodic, and 4T-periodic) in addition to the T-periodic motion. The existence of these types of movements is proved by the section of Poincaré composed of several points (1 point, 2 points, 3 points, and 4 points) and by the shape of the rotor center orbits (Figures 7a–d). For $\overline{\omega} > 4.71$ and from the 4T-periodic motion, the shaft movement becomes chaotic instead of quasi-periodic observed at $\overline{a} = 0.05$. The existence of the chaotic movement is proved by the fractal structure of the points defined in the Poincaré map

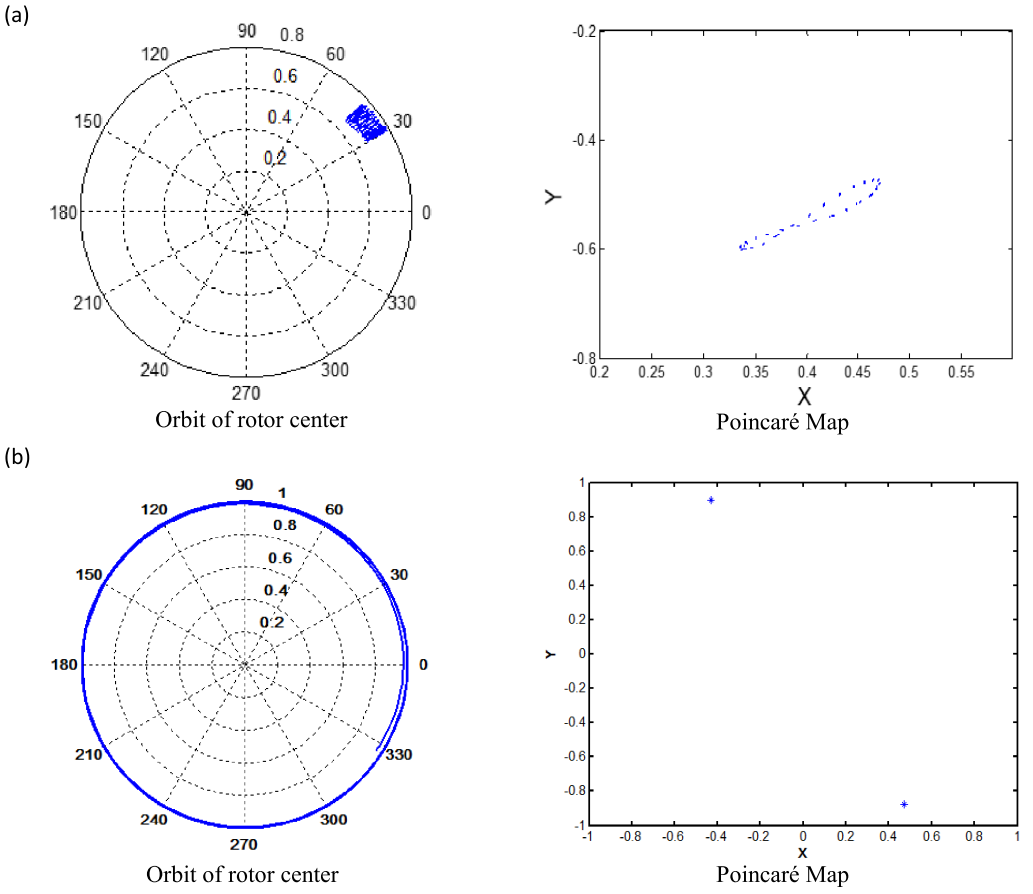

Figure 5. Shaft movement for $\Gamma = 0.015$ and $\overline{a} = 0.05$: (a) quasi-periodic motion at $\overline{\omega} = 11$, (b) 2T-periodic motion with large oscillations at $\overline{\omega} = 15$.

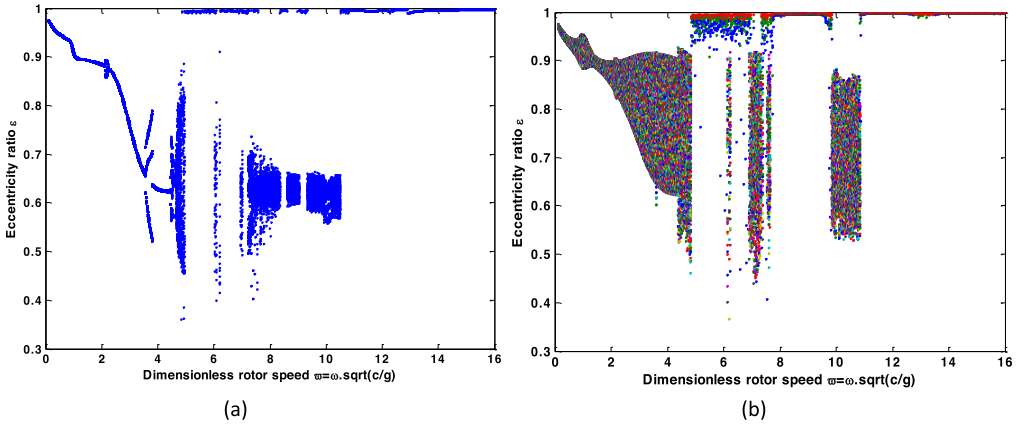

Figure 6. Bifurcation diagram and motion graph for $\Gamma = 0.015$ and $\overline{a} = 0.1$: (a) bifurcation diagram, (b) motion graph.

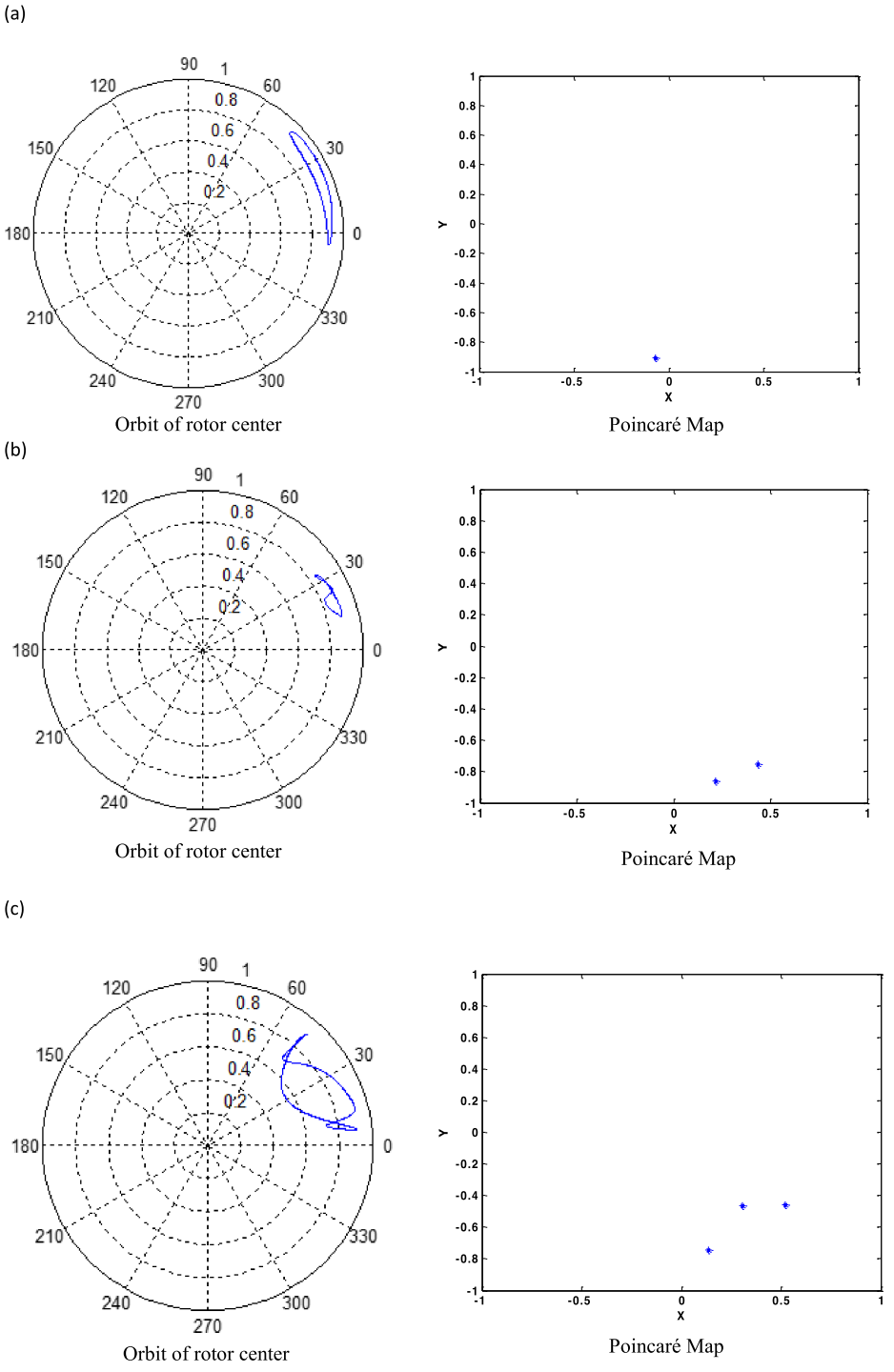

Figure 7. Continued on next page.

(Figure 7e). The chaotic movement covers a large range of speeds $4.71 < \overline{\omega} < 10.49$. Figure 6 shows that during the chaotic motion the rotor center undergoes jumps to a periodic movement

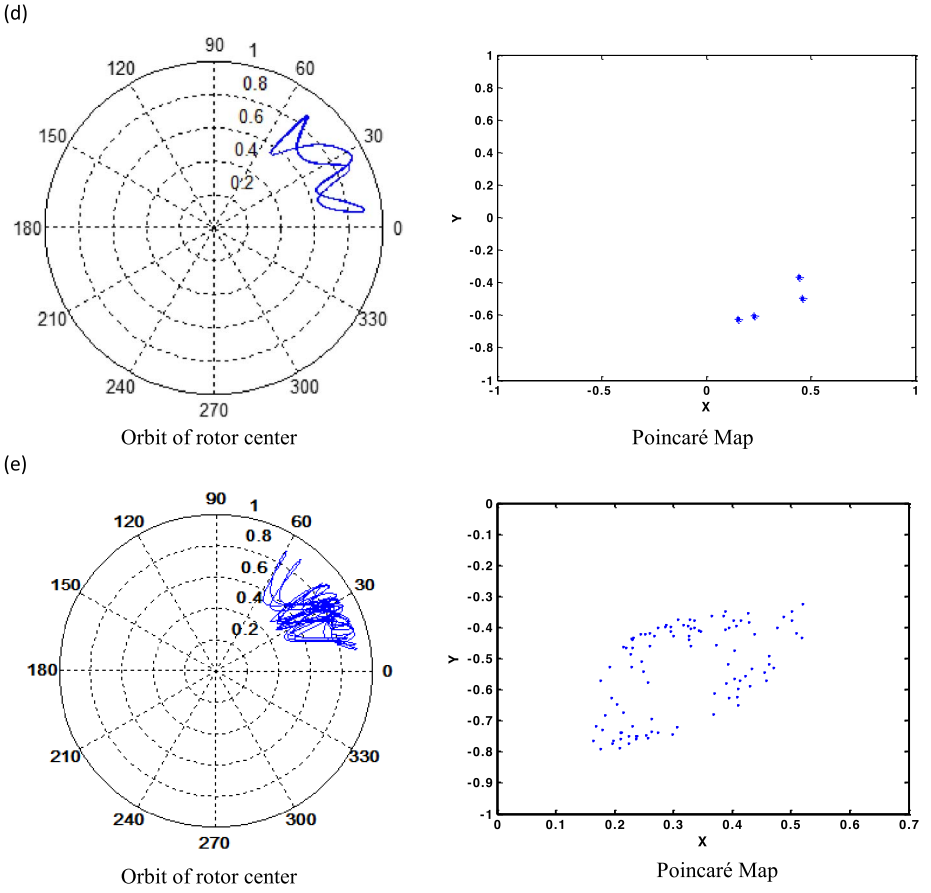

Figure 7 (cont.). Shaft Movement for $\Gamma = 0.015$ and $\overline{a} = 0.1$: (a) T-periodic motion at $\overline{\omega} = 1$, (b) 2T-periodic motion at $\overline{\omega} = 2.2$, (c) 3T-periodic motion at $\overline{\omega} = 3.7$, (d) 4T-periodic motion at $\overline{\omega} = 4.6$, (e) chaotic motion at $\overline{\omega} = 4.8$.

characterized by contact between the shaft and the bearing. These sudden jumps are explained by the fact that during the chaotic motion the rotor center follows orbits of variable amplitudes. When these amplitudes are exceeded at certain operating speeds the amplitude of unstable limit cycles defined between LPC1 and LPC2 in Figure 3(a) for a balanced rotor, in this case, the movement of the shaft center escapes the attraction field of a stable solution. Since the hydrodynamic forces are a direct function of the eccentricity, they increase proportionally with the increase of the amplitude of vibration. When these forces become the highest components of the system, the rotor begins to whip. This phenomenon is shown in Figure 6 during the chaotic movement, by the sudden jumps and the transient contact between the shaft and the bearing.

From $\overline{\omega} > 10.49$, the shaft movement becomes 2T-periodic with large oscillations characterized by contact between shaft and bearing. For the unbalance value $\overline{a} = 0.1$, it is therefore advisable to operate the rotor at speeds below $\overline{\omega} = 4.71$ to avoid any risk of unpredictable contact between the shaft and the bearing. For this unbalance value, if we consider the area where the movement is chaotic as unacceptable operating range, a very important effect of the unbalance on the stability threshold speed is observed for $\Gamma = 0.015$. This effect results in the passage of the stability threshold speed from $\overline{\omega} = 13.9$ for $\overline{a} = 0.05$ to $\overline{\omega} = 4.71$ for $\overline{a} = 0.1$. This means that the stable speed range is shrinking by more than 65% for an unbalance increase of 0.05.

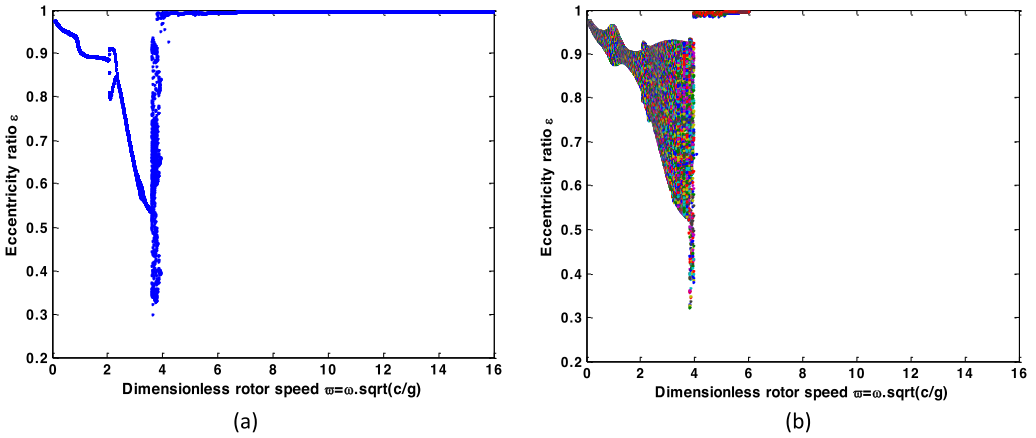

Figure 8. Bifurcation diagram and motion graph for $\Gamma = 0.015$ and $\overline{a} = 0.15$: (a) bifurcation diagram, (b) motion graph.

When the unbalance is increased to a value greater than $\overline{a} = 0.1$, the chaotic oscillations gradually disappear. The movement of the rotor center moves from a chaotic motion to a periodic motion of a large amplitude $\varepsilon \approx 1$ at approximately $\overline{\omega} = 3.91$, as shown in Figures 8 and 9 for unbalance $\overline{a} = 0.15$. The jump point corresponds to the LPC2 bifurcation shown in Figure 3(a). Figures 8 and 9 also show that the motion becomes 2T-periodic in the speed range $2.04 < \overline{\omega} < 2.34$ and quasi-periodic in the vicinity of $\overline{\omega} = 3.05$. Increasing the unbalance from 0.1 to 0.15 clearly reduces the area of chaotic motion that is observed only for $3.63 < \overline{\omega} < 3.91$ at $\overline{a} = 0.15$. The chaotic domain narrowing is explained by the increase of the chaotic orbits' amplitudes under the effect of the increase in unbalance forces. Due to these effects, the amplitudes of the chaotic movements become larger than that of the LPC2 orbit (Figure 3(a)). At this stage, the shaft center movement leaves the field of attraction of stable solutions defined by unstable limit cycles and diverges to a movement with contact between the shaft and the bearing. The stability threshold speed at this unbalance value is approximately $\overline{\omega} = 3.63$.

For an unbalance value $\overline{a} = 0.2$, the movement of the rotor center transits by varying the speed from a T-periodic movement to a 2T-periodic movement, then to a quasi-periodic movement before it undergoes a jump to large oscillations $\varepsilon = 1$ at $\overline{\omega} = 3.37$ (Figure 10). For $\overline{a} > 0.15$, it can be seen that the effect of the unbalance force on the stability threshold and the nature of the movement is relatively small. This can be explained by the disappearance of the chaotic domain, which is very sensitive to the increase of the imbalance.

The case of a moderate bearing parameter $\Gamma = 0.15$ is now considered. This case is characterized by a significantly reduced speed range for the stable supercritical oscillations observed in Figure 2 for the case of a balanced rotor. Figure 11 shows that the increase in rotor imbalance from $\overline{a} = 0.05$ to $\overline{a} = 0.2$ leads to a gradual increase in the amplitude of T-periodic and 2T-periodic oscillations and to the disappearance of the quasi-periodic movement. In addition, this figure shows that the increase in unbalance has a weak effect at moderate bearing parameters $\Gamma = 0.15$. This is deduced by the small reduction in the rate of occurrence of period doubling oscillations and by the small decrease in the critical stability speed. The latter only varies from $\overline{\omega} = 2.82$ for $\overline{a} = 0.05$ to $\overline{\omega} = 2.6$ for $\overline{a} = 0.2$. The jump speed for $\overline{a} = 0.2$ corresponds to the $\overline{\omega}_{\mathrm{EBC}}$ shown in Figure 3(b). This is explained by the fact that at the jump speed the amplitude of the 2T-periodic oscillations is greater than the amplitude of the EBC orbit. For $\overline{a} = 0.05$, the jump speed $\overline{\omega} = 2.82$ is in the speed range $\overline{\omega}_{\mathrm{LPC}} - \overline{\omega}_{\mathrm{EBC}}$, with $\overline{\omega}_{\mathrm{LPC}} = 2.88$ and $\overline{\omega}_{\mathrm{EBC}} = 2.6$. In this speed range, as explained previously in this article, an oscillation of amplitude greater than that of the unstable limit

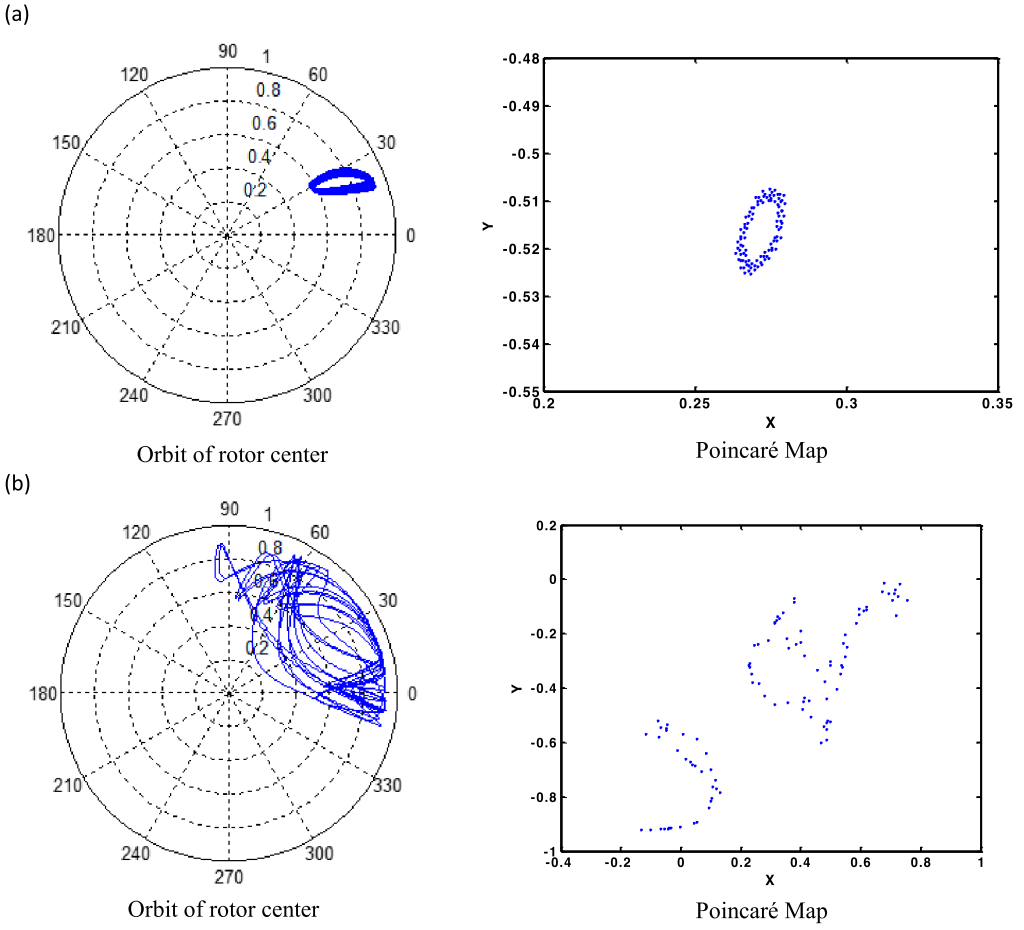

Figure 9. Shaft Movement for $\Gamma = 0.015$ and $\overline{a} = 0.15$: (a) quasi-periodic motion at $\overline{\omega} = 3.2$, (b) chaotic motion at $\overline{\omega} = 3.65$.

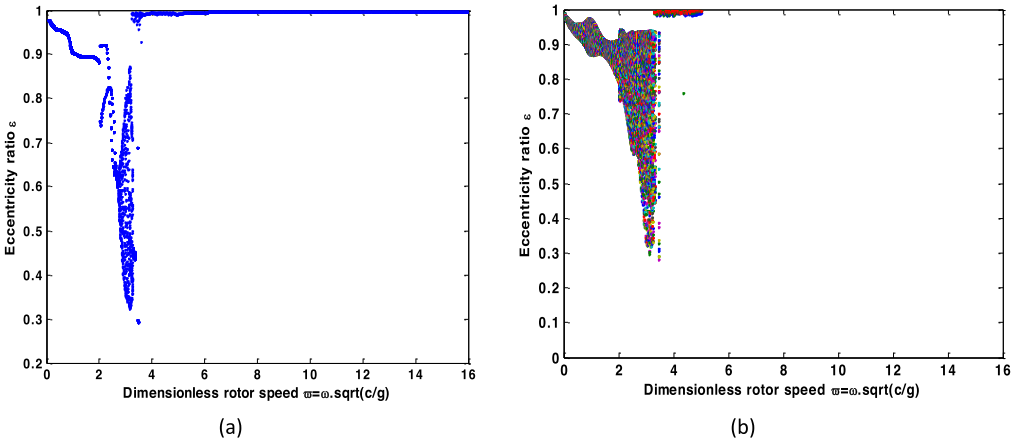

Figure 10. Bifurcation diagram and motion graph for $\Gamma = 0.015$ and $\overline{a} = 0.2$: (a) bifurcation diagram, (b) motion graph.

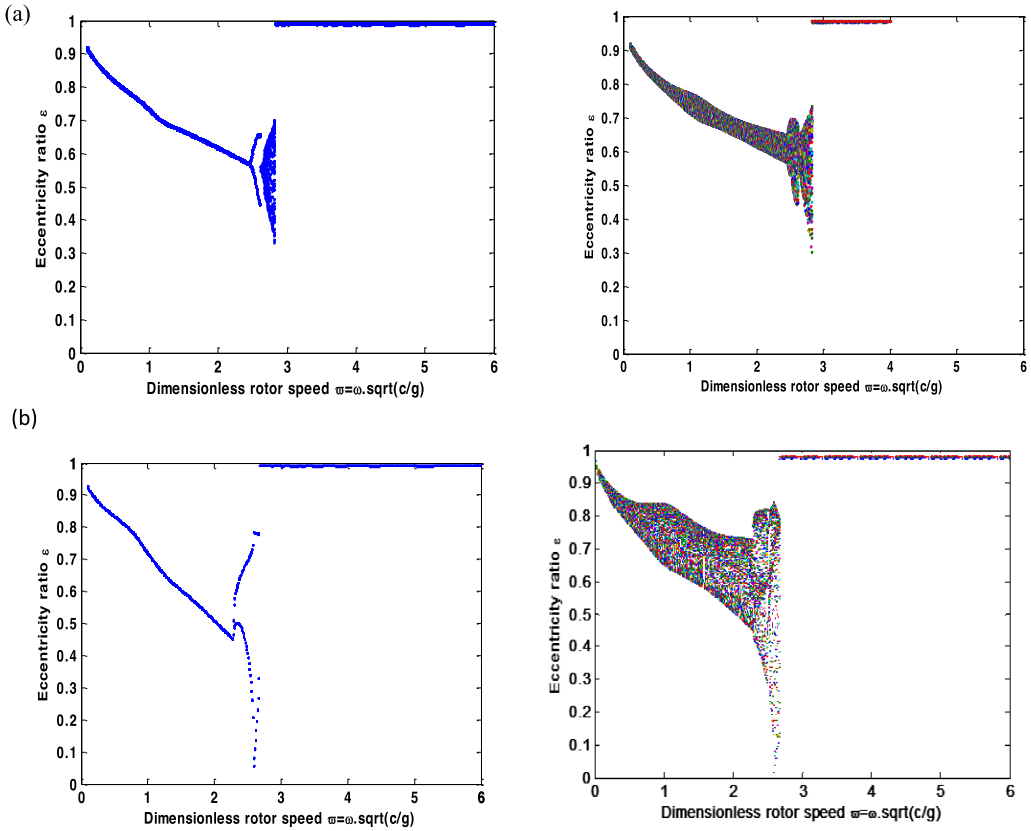

Figure 11. Effect of increasing unbalance from $\overline{a} = 0.05$ to $\overline{a} = 0.2$ on the shaft motion for $\Gamma = 0.15$: (a) bifurcation diagram and motion graph for $\Gamma = 0.15$ and $\overline{a} = 0.05$, (b) bifurcation diagram and motion graph for $\Gamma = 0.15$ and $\overline{a} = 0.2$.

cycles can make the rotor jump at a large limit cycle movement, which explains the jump speed for $\overline{a} = 0.05$.

The last case considered corresponds to the bearing parameter $\Gamma = 1.5$. In this case, the stability threshold speed is detected at a Hopf bifurcation $\overline{\omega}_H = 2.71$ as shown in Figures 2 and 3(b) for the case of a balanced rotor. In the case of an unbalanced rotor and for $\overline{a} = 0.05$ (Figure 12), the movement becomes T-periodic up to $\overline{\omega} = 2.65$ which is close to that corresponding to Hopf's bifurcation. Then the oscillations become 2T-periodic with an amplitude that tends rapidly to an eccentricity close to one, whereas for $\overline{a} = 0.2$, the jump speed is close to the speed $\overline{\omega}_{\text{EBC}} = 2.45$ for the case of a balanced rotor (Figure 3(b)). This jump is explained by the increase of the T-periodic orbits' amplitudes under the effect of the unbalance force increase. Due to this effect, the amplitudes of T-periodic movements become larger than that of the EBC orbit (Figure 3(b)). At this stage, the shaft center movement leaves the attraction field of stable solutions and diverges to an oscillation with contact between the shaft and the bearing. This result further justifies the relationship to be determined between the bifurcation diagram of a balanced rotor and the dynamic behavior of an unbalanced rotor. This relation is considered among the contributions of this study in the field of rotor dynamics. The effect of increasing the unbalance from 0 to 0.2, for this bearing parameter, is observed essentially by the increase of the T-periodic oscillation's amplitudes.

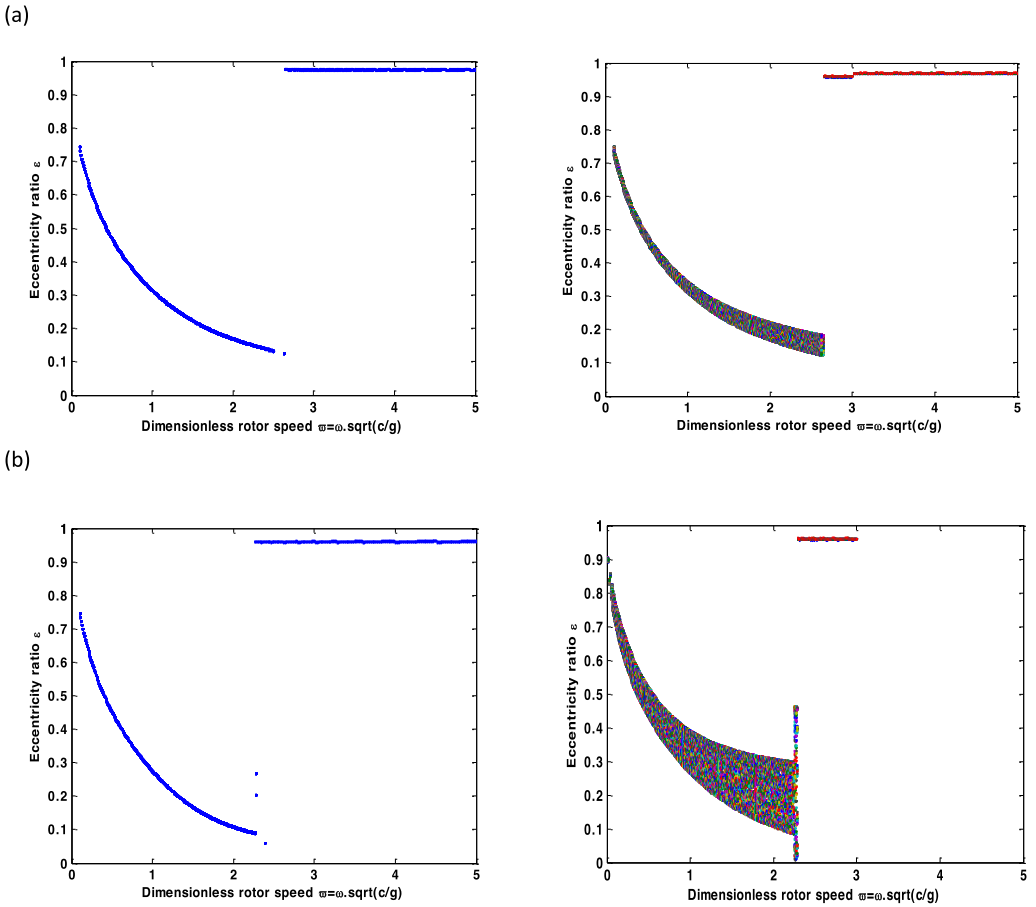

Figure 12. Effect of increasing unbalance from $\overline{a} = 0.05$ to $\overline{a} = 0.2$ on the shaft motion for $\Gamma = 1.5$: (a) bifurcation diagram and motion graph for $\Gamma = 1.5$ and $\overline{a} = 0.05$, (b) bifurcation diagram and motion graph for $\Gamma = 1.5$ and $\overline{a} = 0.2$.

In this paper, a model with two degrees of freedom is used to study the effect of unbalance on the movement of a rotor with short bearings at different rotational speeds. The bifurcation diagrams for a balanced rotor, determined by numerical continuation, have been found very useful for predicting the admissible operating range. For low bearing parameters, which correspond to low oil viscosity or high static loads, a wide range of permissible operating speeds have been found. This wide range is considered possible only for a small rotor imbalance. This domain is reduced to less than half for medium and high unbalance values. The speed domain reduction is justified by the presence of a narrow domain of unstable limit cycles between LPC1 and LPC2 and by the appearance of chaotic motion for the medium values of unbalance. This type of movement appeared because of the low hydrodynamic forces (low viscosity of the oil) which characterize the low bearing parameters. These forces cannot control the rotor movement under the unbalance force action, which leads to a domain of chaotic motion and sudden jump. When the unbalance increases, the chaotic domain completely disappears. The latter case is due to the increase in hydrodynamic forces as a function of the increase in oscillation amplitudes under the unbalance force effect. Due to these effects, the movement amplitudes become larger than of the LPC2 orbit. At this stage, the shaft comes into contact with the bearing. This causes a high

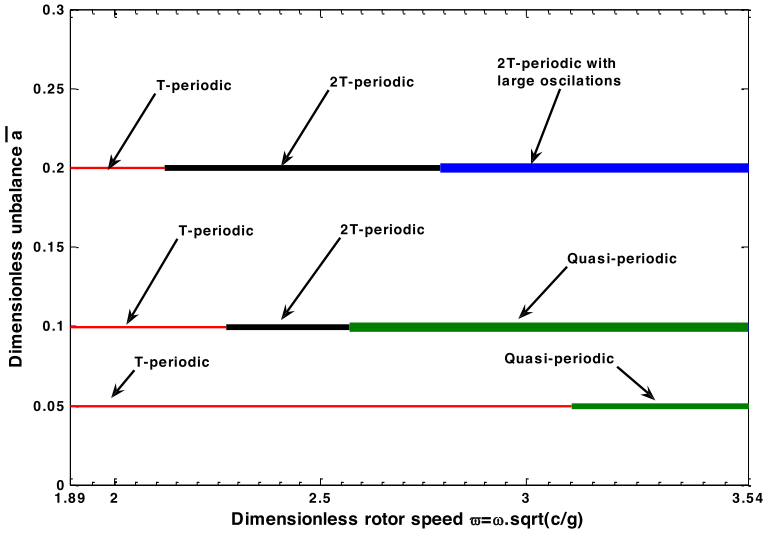

Figure 13. Diagram of movements determined numerically in this paper for a rotor with short bearings and for unbalance values $\overline{a} = 0.05$, 0.1 and 0.2.

reduction in the operating range. For moderate and high bearing parameters, the stable speed range is almost independent of the unbalance level. Furthermore, the amplitude of the stable oscillations increases with unbalance progressive augmentation. This is explained by the low-speed range of the unstable limit cycles existence and by the important values of the hydrodynamic forces for these parameters, which prevent the appearance of the chaotic domain.

5. Discussion

This section presents a comparative study between the results of this article and those published in previous studies. Also, the contributions of this article are discussed in relation to those in previous literature.

The chaotic motion at low values of the bearing parameter was signaled by several studies [14–17, 21]. These studies, which were performed on an unbalanced rigid rotor supported by short bearings, also indicated that chaotic motion is obtained for moderate unbalance values. The published theoretical findings are consistent with the findings found in this paper.

An experimental study [14] yielded bifurcation diagrams at a low value of a bearing parameter $\Gamma = 0.074$ and for a ratio $L/D = 0.25$ which is suitable for modeling by a short bearing. These diagrams are established in a speed range $1.89 < \overline{\omega} < 5.67$ and for unbalance values $\overline{a} = 0.05, 0.1, 0.2, 0.3, 0.35$. A good correspondence between the numerical and experimental results was found for the speed range $1.89 < \overline{\omega} < 3.54$ and for unbalance values $\overline{a} = 0.05, 0.1, 0.2$ (Figures 13 and 14).

The movements observed experimentally and numerically are similar with reasonable shifts in the speeds of change of the movement's nature. These shifts are observed especially for the case of a high unbalance value $\overline{a} = 0.2$. The observed offsets could be explained by the variation of the oil viscosity during operation and the misalignment of bearings that are not taken into account in the modeling.

In previous research [14–16], the unbalanced rotors considered have characteristics corresponding to a rotor-bearing system of a low bearing parameter whose Hopf bifurcation is supercritical. The contribution of this study is the prediction of rotor motion for various geometries

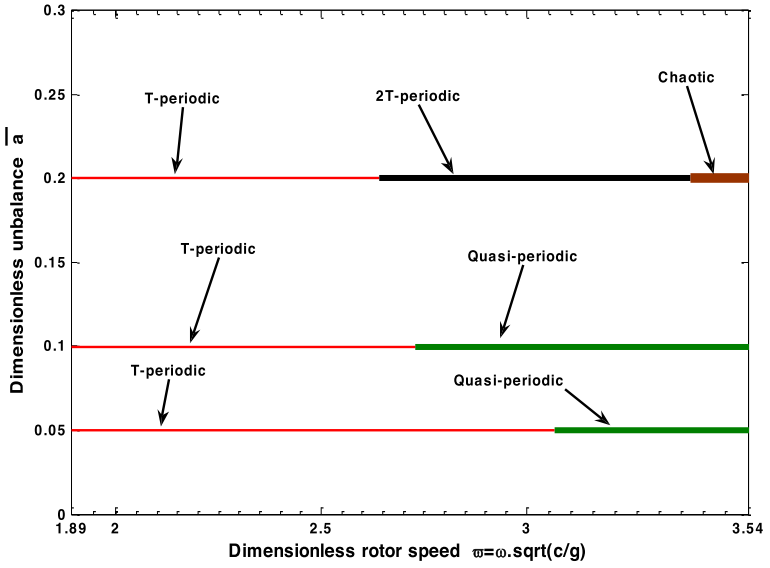

Figure 14. Diagram of movements determined experimentally in [14] for a rotor with short bearings and for unbalance values $\overline{a} = 0.05$, 0.1 and 0.2.

of the rotor-bearing system. On the other hand, we have proposed in this paper a motion graph able to visualize the appearance of the rotor oscillations. Also, this study identified the imbalance effect on rotor motion and on the nonlinear stability threshold speed using two different numerical methods: the numerical continuation method and the numerical integration method. In addition, in this study, we have explained the effect of bearing geometry, oil viscosity, and the speed range of unstable limit cycles existence on rotor motion, stability threshold speed, the whirl speed and the occurrence of chaotic motion.

The major contribution of this paper is the establishment of a relationship between the bifurcation diagram of a balanced rotor and that of an unbalanced rotor: the relation between the speed range of unstable limit cycles existence, the whirl speed, and the occurrence of chaotic motion. Such a relationship was not determined or investigated in previous articles. It allows deeper comprehension of the dynamic behavior of the rotor with unbalance defect and to improve the design of bearing rotor systems.

6. Conclusion

In this paper, a two degree of freedom model is used to study the effect of unbalance on shaft motion at different rotational speeds and for a short journal bearing system. Bifurcation diagrams for a balanced rotor are determined by numerical continuation while the bifurcation diagrams of an unbalanced rotor are determined by numerical integrations. For a low bearing parameter, which corresponds to a low oil viscosity or high static loads, a wide range of safe operating speeds is found for low unbalance value. This wide domain is considered very sensitive to the increase of the unbalance. The latter is reduced by at least half for medium and high value unbalance. The reduction of the speed domain is justified by the presence of a narrow domain of unstable limit cycles between LPC1 and LPC2 and by the appearance of chaotic motion for the medium values of unbalance. However, it has been found for the moderate and high bearing parameters that the stable speed range is almost independent of the level of imbalance. For these parameters, the unbalance effect is observed by the increase of the amplitudes of the stable oscillations.

This is explained by the low-speed range of existence of unstable limit cycles and by the important values of the hydrodynamic forces for these parameters which avoid the appearance of the chaotic domain. This study allowed to establish a relationship between the bifurcation diagram of a balanced rotor and that of an unbalanced rotor. Moreover, it was possible to judge that the use of a rotor-bearing system characterized by a moderate or elevated bearing parameter is more adequate in case of unbalance defect to avoid sudden jump, unpredictable contact, and unexpected narrowing of the safe operating speed range.

Conflict of interest

The author declares that they have no conflict of interest.

Funding

This research received no specific grant from any funding agency in the public, commercial or not-for-profit sectors.

References

[1] M. Gardner, C. Myers, M. Savage, C. Taylor, "Analysis of limit-cycle response in fluid-film journal bearings using the method of multiple scales", *Q. J. Mech. Appl. Math.* **38** (1985), p. 1258-1264.
[2] C.-J. Meyers, "Bifurcation theory applied to oil whirl in plain cylindrical journal bearings", *J. Appl. Mech.* **51** (1984), p. 244-250.
[3] J.-K. Wang, M.-M. Khonsari, "On the hysteresis phenomenon associated with instability of rotor-bearing systems", *J. Tribol.* **128** (2005), p. 188-196.
[4] J.-S. Guo, "Characteristics of the nonlinear hysteresis loop for rotor-bearing instability", 1995, Dissertation, Case Western Reserve University.
[5] A. Boyaci, H. Hetzler, W. Seemann, C. Proppe, J. Wauer, "Analytical bifurcation analysis of a rotor supported by floating ring bearings", *Nonlinear Dyn.* **57** (2009), p. 497-507.
[6] M. Chouchane, R. Sghir, "Stability and bifurcation analysis of a flexible rotor-bearing system by numerical continuation", in *10th International Conference on Vibrations in Rotating Machinery* (London), Woodhead Publishing, 2012.
[7] R. Sghir, M. Chouchane, "Prediction of the nonlinear hysteresis loop for fluid-film bearings by numerical continuation", *Proc. Inst. Mech. Eng. C* **229** (2015), p. 651-662.
[8] R. Sghir, M. Chouchane, "Nonlinear stability analysis of a flexible rotor-bearing system by numerical continuation", *J. Vib. Control* **22** (2016), p. 3079-3089.
[9] F.-F. Ehrich, "Observations of subcritical superharmonic and chaotic response in rotordynamics", *J. Vib. Acoust.* **114** (1992), p. 93-100.
[10] M. Russo, R. Russo, "Parametric excitation instability of a rigid unbalanced rotor in short turbulent journal bearings", *Proc. Inst. Mech. Eng. C* **207** (1993), p. 149-160.
[11] F.-F. Ehrich, "Some observations of chaotic vibration phenomena in high-speed rotordynamics", *J. Vib. Acoust.* **113** (1991), p. 50-57.
[12] G. Genta, C. Delprete, A. Tonoli, R. Vadori, "Conditions for noncircular whirling of nonlinear isotropic rotors", *Nonlinear Dyn.* **4** (1993), p. 153-181.
[13] S.-K. Choi, S.-T. Noah, "Mode-locking and chaos in a jeffcott rotor with bearing clearances", *J. Appl. Mech.* **61** (1994), p. 131-138.
[14] G. Adiletta, A.-R. Guido, C. Rossi, "Chaotic motions of a rigid rotor in short journal bearings", *Nonlinear Dyn.* **10** (1996), p. 251-269.
[15] G. Adiletta, A.-R. Guido, C. Rossi, "Nonlinear dynamics of a rigid unbalanced rotor in journal bearings. Part I: theoretical analysis", *Nonlinear Dyn.* **14** (1997), p. 57-87.
[16] G. Adiletta, A.-R. Guido, C. Rossi, "Nonlinear dynamics of a rigid unbalanced rotor in journal bearings, Part II: experimental analysis", *Nonlinear Dyn.* **14** (1997), p. 157-189.
[17] G. Adiletta, E. Mancusi, S. Strano, "Nonlinear behavior analysis of a rotor on two-lobe wave journal bearings", *Tribol. Int.* **44** (2011), p. 42-54.
[18] F. Chu, Z. Zhang, "Periodic, quasi-periodic and chaotic vibrations of a rub-impact rotor system supported on oil film bearings", *Int. J. Eng. Sci.* **35** (1997), p. 963-973.

[19] P. Varney, I. Green, "Nonlinear phenomena, bifurcations, and routes to chaos in an asymmetrically supported rotor–stator contact system", *J. Sound Vib.* **336** (2015), p. 207-226.
[20] J. Hong, P. Yu, D. Zhang, Y. Ma, "Nonlinear dynamic analysis using the complex nonlinear modes for a rotor system with an additional constraint due torub-impact", *Mech. Syst. Signal Process.* **116** (2019), p. 443-461.
[21] R.-D. Brown, G. Drummond, P.-S. Addison, "Chaotic response of a short journal bearing", *Proc. Inst. Mech. Eng. J.* **214** (2000), p. 387-400.
[22] H.-K. Yadav, S.-H. Upadhyay, S.-P. Harsha, "Study of effect of unbalanced forces for high speed rotor", *Proc. Eng.* **64** (2013), p. 593-602.
[23] C.-K. Chen, H.-T. Yau, "Bifurcation in a flexible rotor supported by short journal bearings with nonlinear suspension", *J. Vib. Control* **7** (2001), p. 653-673.
[24] H. Ma, H. Li, H. Niu, R. Song, B. Wen, "Nonlinear dynamic analysis of a rotor-bearing-seal system under two loading conditions", *J. Sound Vib.* **332** (2013), p. 6128-6154.
[25] H. Ma, X. Li, H. Zhao, H. Niu, B. Wen, "Effects of eccentric phase difference between two discs on oil-film instability in a rotor-bearing system", *Mech. Syst. Signal Process.* **41** (2013), p. 526-545.
[26] H. Ma, H. Li, H. Niu, R. Song, B. Wen, "Numerical and experimental analysis of the first-and second-mode instability in a rotor-bearing system", *Arch. Appl. Mech.* **84** (2014), p. 519-541.
[27] H. Ma, X. Li, H. Niu, B. Wen, "Oil-film instability simulation in an overhung rotor system with flexible coupling misalignment", *Arch. Appl. Mech.* **85** (2015), p. 893-907.
[28] J. Frene, D. Nicolas, B. Degueurce, D. Berthe, M. Godet, *Hydrodynamic Lubrication Bearings and Thrust Bearings*, Elsevier, Amsterdam, 1997.
[29] A.-H. Nayfeh, B. Balachandran, *Applied Nonlinear Dynamics*, WILEY-VCH Verlag GmbH & Co. KGaA, Weinheim, 1995.
[30] R. Seydel, "Nonlinear computation", *J. Franklin Inst.* **334** (1997), p. 1015-1047.
[31] Y.-A. Kuznetsov, *Elements of Applied Bifurcation Theory*, Springer-Verlag, New York, 1998.
[32] A. Dhooge, W. Govaerts, Y.-A. Kuznetsov, "Matcont: A Matlab package for numerical bifurcation analysis of ODEs", *ACM Trans. Math. Softw.* **29** (2003), p. 141-164.
[33] Y. Hori, T. Kato, "Earthquake-induced instability of a rotor supported by oil film bearings", *J. Vib. Acoust.* **112** (1990), p. 160-265.